Journal of Magnetic Resonance 341 (2022) 107233

Contents lists available at ScienceDirect

Journal of Magnetic Resonance

journal homepage: www.elsevier.com/locate/jmr

Net-phase flow NMR for compact applications

Pedro F. Silva [1], Mehrdad Alinaghian Jouzdani [1], Miguel Condesso, Andrea C. Hurtado Rivera, Mazin Jouda, Jan G. Korvink *

Karlsruhe Institute of Technology (KIT), Institute of Microstructure Technology, Karlsruhe 76131, Germany

ARTICLE INFO

Article history:
Received 3 November 2021
Revised 5 March 2022
Accepted 3 May 2022
Available online 30 May 2022

Keywords:
Compact flow NMR
Net-phase encoding
Planar front-end
Biplanar shims
Stripline

ABSTRACT

The net phase of the NMR signal is proposed as a robust mechanism for the encoding of fluid flow velocity into phase, showing local bijectivity. While magnitude-based or imaging-based methods suffer from loss of signal, by increasing the flow rate, the present method enables us to maintain the high SNR even for the case of fast flow. In addition, it is shown that a well-engineered flow channel is also necessary, which is not the case for traditional cylindrical flow channels. In this contribution, we report on implementing this approach in a low-cost NMR-based flowmeter for use in a low field (1 T) setting, for example, for monitoring reaction flow industrial processes.

1. Introduction

Even before the first report on magnetic resonance imaging in 1972 [9,11], it was realised that motional sensitivity in nuclear magnetic resonance could be used to measure flow velocity [12]. This new ability, including the well-known spectroscopic identification of most fluids, the geometric resolution of any propriety (i.e. MRI), and less known abilities like NMR thermometry or pressure quantification, shows significant potential in the implementation of new combined flowmeter/spectrometer solutions. Beyond these unique abilities, NMR is one of the least invasive and demanding approaches when compared to competing non-invasive technologies, requiring no specific flow-channel (unlike Coriolis flowmeters), no patterning of the inner walls of a flow channel (unlike most thermal flowmeters), the use of translucent/-conductive fluids (unlike optical and electromagnetic flowmeters), or the introduction of supporting elements (unlike in particle imaging velocimetry).

Nevertheless, and despite interim advances in state-of-the-art of magnetic resonance and flow visualisation, these techniques are not in widespread use in industry [1], where they could be used to observe and optimize inline chemical engineering processes. The aim of this work is to establish a new approach to NMR-based flow measurement which facilitates low-cost applications for non-invasive flow monitoring.

NMR can be employed in a variety of ways to study several complex features of flows: laminar, turbulent, or multiphase behaviour, in aerosol, slurry, or emulsion colloids, all in a non-invasive manner [7]. However, when attempting to quantify flow dynamics, most current approaches come at the cost of the loss of other spectroscopic information and are generally divided into imaging techniques, and one-dimensional responses of a local or a displaced sample.

Imaging methods, due to exceptional advances, are now able to generate a wealth of 4D information on the flow [4], which can further be made species-selective, or even temperature and pressure dependent. However, these are complex to achieve and require either high-performance instrumentation or simplistic flow conditions, so as to offset the SNR loss that comes with the encoding process, and the spatial division of the flow field into higher resolution voxels. The latter is intrinsically linked to the reduced statistical certainty in the subset that constitutes a voxel, a major limitation in NMR. Furthermore, imaging encoding and readout require moderate to long acquisition times [8], depending on the desired spatial resolution, which prove to be limiting for fast flow rates or when quick probing rates are necessary.

Another approach to flow analysis and the one taken here, consists of reducing the intrinsic information obtained from constrained, repeatable, and calibrated flow conditions, such as laminar flow in a pre-defined channel, to which imaging techniques afford no extra information. If the flow channel is pre-engineered and well-characterised, this allows for a repeatable laminar flow profile and consistent behaviour over a range of flow

* Corresponding author.
E-mail address: jan.korvink@kit.edu (J.G. Korvink).
[1] Authors contributed equally.

https://doi.org/10.1016/j.jmr.2022.107233
1090-7807/

speeds that include a predefined calibration point. Given these presuppositions, one can correlate the spatially extended flow measurement with a single point, one-dimensional response to the channel's flow. This approach is commonly used to encode the NMR signal's magnitude with the flow information, with or without time resolution. Local techniques [17,14] use a single coil where either the sensitive volume is saturated and the measured signal is from freshly polarised spins that have entered the measurement volume, or the sensitive volume is excited and the signal decay is exacerbated as excited spins flow away. Non-local methods are based on different readouts of a given sample plug excited with one coil and detected with another downstream, in a time-of-flight manner [13]. It becomes clear that the aforementioned techniques intrinsically suffer from two major limitations: their dimension-linked response, and sub-optimal acquisition. The former arises from the need to have a significant signal magnitude change within the residence time of the fluid plug in the coil, which ultimately limits the measurable range of a particular setup. Furthermore, the acquisition procedure requires either a significant delay time (e.g. the time-of-flight), or an acquisition that spans a significant signal decay (from a high to a low amplitude), which degrades the SNR of the measurement. So, in contrast to reports in the literature, in which flow rate is correlated with the magnitude of the signal, [10,5], leading to loss of signal for a range of flow rates, this study records the relationship between the flow rate and phase of the signal. This techniques enables one to perform a measurement with maximum signal and keep SNR high, even for the case of fast/slow flows. In an effort to combine the benefits of *flow-adjustable* phase-encoding procedures used for flow-imaging, and the low-information, yet statistically significant *one dimensional response* of portable systems, a simple front-end is proposed in Section 3, implementing the concept developed in Section 2. This new approach to flow velocimetry, despite initial limitations, achieves measurement precision matching that of the NMR measurement itself. Experimental results are shown in Section 4 and further interpreted in Section 5, dissecting the strengths of the technique, and exploring the potential for its improvement.

2. Theoretical setup

Given the objective of measuring engineering flows in a non-invasive manner, the authors took a top-down approach to the design of an NMR front-end, so as to maximise flow sensitivity. Phase encoding was found to be an optimal technique to measure flow, as it introduces information in an often disregarded dimension of 1D NMR, namely the signal's phase, rather than its amplitude. Unlike magnitude-encoding methods, which, by definition, require a change in magnitude away from the optimum, thus degrading overall SNR, phase can be registered at the optimal signal strength. The phase encoding approach was thus used to encode flow, as an $\mathbb{R} \rightarrow \mathbb{R}$ mapping function, to best leverage fast NMR measurements, at fast probing rates, in a harsh environment, and at low cost, for which SNR will become the precision bottleneck. Consider the incremented phase encoded into a spin ensemble after a bipolar gradient G_v is applied, for a total time T_{enc}, on a fluid element moving at velocity v_0 and accelerating at a_0:

$$\phi = \int_0^{T_{enc}} \gamma G(t) \cdot r(t)\, dt \approx \frac{-\gamma G_v T_{enc}^2}{4}\left(v_0 + \frac{1}{2}a_0 T_{enc}\right) = k_{enc}\overline{v} \qquad (1)$$

The encoded phase will be well-resolved for each spin but, without imaging techniques, only its weighted contribution will be measured in a real flow. The overall response of plug flow, assuming a uniform encoding gradient, would match the theoretical ideal without convolution with a velocity profile, but is not achievable in generalised flow setups. Conversely, common setups use a cylindrical tube for the flow, which performs sub-optimally due to the sharp velocity distribution introduced by no-slip conditions at the tube boundary. Attempting to reduce this limitation, one could remove wall effects by measuring only the centre of the channel, to the detriment of SNR, or by extending the channel width sufficiently beyond the measurement region, thereby achieving an approximately two-dimensional flow profile. The net-phase of the signal consisting of the sum of all spins, each encoded with a velocity-dependent phase, is shown in Fig. 1.

The approach shown in Fig. 1 maintains a coherent net phase, allowing for a non-zero total signal even for large velocity ranges. Furthermore, whereas the encoding k_{enc} can be adjusted for cylindrical flow to allow for a non-zero amplitude, these show much faster phase wrapping, which, due to non-bijectivity, only allow for the measurement of much slower varying flows. Furthermore, a 2D flow allows for a higher phase encoding value per k_{enc}, which will prove beneficial below. Being able to express the net response as a function of $k_{enc}\overline{v}$ introduces a degree of adjustment of the technique to varying flow ranges, unlike other non-imaging methods. This ultimately shifts the limitation of the technique to the phase encoding process (sequence and gradients), which determines k_{enc}, instead of to the front-end itself (flow chamber and Rx/Tx coils). Having established the ability to measure a fluid across a large phase range, we next have to define the optimisation functional for the desired measurement. Aiming for a high precision measurement of a laminar flow, the Q in a well-defined channel with section A is:

$$\begin{aligned} \mathrm{SNR}_Q &= \frac{Q}{\sigma_Q} = \frac{A\overline{v}}{A\sigma_{\overline{v}}} = \frac{k_{enc}\overline{v}}{k_{enc}\frac{d\overline{v}}{d\phi_{2-1}}\sigma_{\phi_{2-1}}} \\ &= k_{enc}\overline{v}\mathrm{SNR}_0\sqrt{\frac{M^2}{M^2+1}}\frac{d\phi_{2-1}}{d(k_{enc}\overline{v})} \end{aligned} \qquad (2)$$

Here SNR_0 is the signal-to-noise ratio of the stationary measurement, M is the ratio of the SNRs after and before encoding, and $d\phi_{2-1}$ is the phase difference between two consecutive acquisitions. This formula leads to the well-known closed-form for the SNR of a flow measurement in a plug flow regime ($\phi = k_{enc}v, \overline{v} = v, M = 1$), usually approximated well within a single imaging voxel, of:

$$\mathrm{SNR}_Q = \frac{\overline{v}}{\sigma_{\overline{v}}} = \frac{k_{enc}\overline{v}}{\sigma_{\phi_{2-1}}} = k_{enc}\overline{v}\frac{\mathrm{SNR}_0}{\sqrt{2}} \qquad (3)$$

While the method could be expanded to infer the desired flow measurement from *both* the phase and magnitude changes introduced by a bipolar gradient, the statistical significance of the magnitude variation is small (due to an equally small relative variation) and has been seen to be far less robust w.r.t. experimental variations. Eq. (3) is plotted for three flow responses to a bipolar gradient (plug, 2D, and cylindrical flow) in Fig. 2.

Despite the promising framework of the method, its limitations must be taken into consideration when it is implemented for varying configurations. The 'lower bound' of the method, at low velocities, is the inability to generate a sufficient k_{enc}, due to a limited current supply, thermal concerns in the gradient, or a T_{enc} rivalling the measurement time or T_2^*, which imparts a small, statistically non-significant phase, meaning that flow cannot be discerned. On the other hand, slow measurable flows require the application of the strongest gradient possible for a short period of time (to achieve the large k_{enc} value necessary), to avoid leading to loss of signal due to diffusion.

Despite the increasing statistical significance of measurements at large $k_{enc}\overline{v}$, other measurement-detrimental effects will come into play, creating a finite span of the flow measurement, and therefore the method's 'upper bound'. For high velocities, and as seen in this manuscript, both physical and information-limiting effects come into play. Despite an easier path towards increasing

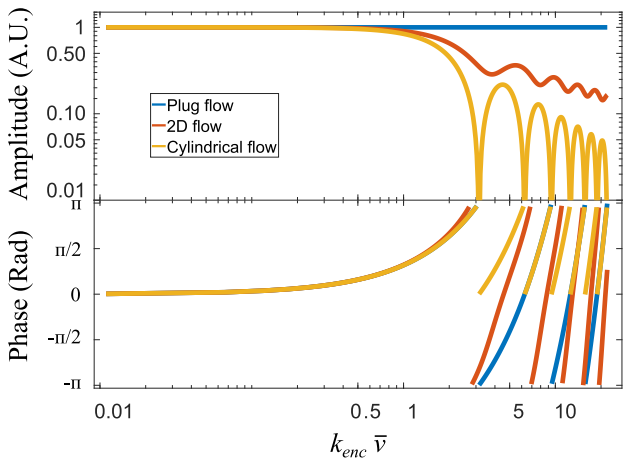

Fig. 1. Magnitude and phase response of the NMR signal from of a phase-encoded fluid with average velocity $\overline{v}$. Results shown for three flow conditions: $v = \overline{v}$, $v = 1.5\,\overline{v}\,(1 - z^2/z_0^2)$ and $v = 2\,\overline{v}\,(1 - r^2/r_0^2)$, respectively.

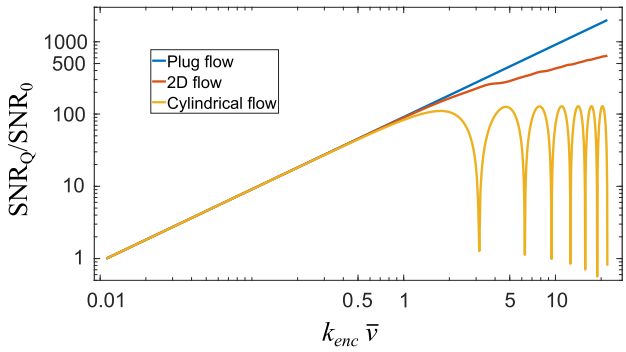

Fig. 2. Dependence of the NMR flow measurement's SNR on average flow velocity and encoding intensity k_{enc}, for three distinct flow conditions.

the injected phase (i.e. a large velocity reduces the encoding time and gradient strength necessary), a large encoding value requires a sufficient flow range within which the mapping remains bijective, so that a local phase-to-flow correspondence can be achieved. This flow range will become prohibitively narrow as the wrapping frequency increases, as the variation within the bijective domains becomes comparable to that of effects stemming from non-linear gradient terms, or from sharp time variations in the flow. At the same time, the expected phase response requires that the flow retains its near-2D laminar flow profile, which is not guaranteed as Reynold's numbers and entry/exit lengths increase with increasing flow speeds. This deviation, while possibly information-preserving, is outside of the scope of this manuscript. Similarly, and depending on hardware used, faster flows mean that the fluid has a shorter residence time inside the measurable or encodable volumes at play, which either requires shortening the experiment, or the introduction of further deviations from the model.

3. Flowmeter front-end

Given the promising theoretical results shown in Section 2, our objective was to design a simple flow channel prototype that generates the desired near-2D laminar velocity profile with the less possible deviation within the volume of interest (VOI). To achieve this, a top-down development procedure was followed to obtain a compatible relationship between the flow channel, the sensitivity profile of the detector, and the selective shim-set. The entire system was designed to be inserted in a 15 mm gap permanent magnet, for operation under field conditions, and thus the sensitive VOI was set as a rectangular prism of dimensions 3 × 10 × 10 mm at the centre of the volume containing all the relevant coils of 15 × 57 × 60 mm. Components of the device and parameters of the employed pulse sequence are listed in Table 1.

3.1. Flow channel

The total length of the flow measurement chamber consisted of the 10 mm length of the VOI, and the entrance length necessary for the flow to develop. Within the dimensional constraints imposed by the coils, the width was increased as much as possible, so as to best approximate a 2D flow profile along the 10 mm width of the VOI. The coils also constrained the design and positioning of the inlet and outlet. The final design of the flow channel, seen in Fig. 3, resulted in a chamber size of 27x19x3 mm, and makes use of all the available space within the measurement coil (shown in Fig. 7). Following standard planar fabrication techniques, the flow channel was fabricated using three laser-cut PMMA pieces, glued together with UV-curable adhesive (Dymax 1187-M, Dymax Europe GmbH).

The expected near-2D laminar velocity profile and the streamlines are shown within the flow channel design in Fig. 3. In order to verify the behavior of the flow, and its velocity profile, at different mass flow rates, Computational Fluid Dynamics (CFD) simulations were performed using a commercial FEM solver (COMSOL Multiphysics, COMSOL AB). In these, the Navier-Stokes equations were solved for incompressible flow in the laminar regime with a no-slip boundary condition at the walls. The mass flow rate at the inlet was varied between 0.1 kg/h and 2.0 kg/h. The numerical results are in a good comparison with the expected velocity profile within the VOI up to a certain mass flow rate, after which recirculation effects became dominant, as shown in Fig. 4. At this point, the phase behaviour was expected to drastically deviate from the one proposed by the framework, showing an implementation-dependent upper bound to the measurable flow rates. These results were experimentally confirmed in Section 4.

3.2. Rx and Tx coils

Having generated a volume where the velocity matched the desire profile, we selected this volume as the source of signal. This was possible through the design of the detection coil. The use of a stripline geometry allowed to access a large volume enclosed by the measurement coil, unlike what would have been possible for common resonator geometries. The system is described in [18]. The narrow, most sensitive section of the stripline, achieved an optimal total response from the VOI, with a 7 mm width and 10 mm length, and was seen to have a higher sensitivity to the spins localised at the centre, further emphasising the volume that best represented the desired near-2D flow, see Fig. 5.

3.3. Shim set

The use of the system in a permanent magnet setup necessitated the need for shim coils. Given the simplicity of the two-magnet gap system, only small high order contributions to inhomogeneity are expected and thus a second-order shim set was developed. Active shimming systems employ a set of coils capable of producing an orthogonal basis of the B_z component of the magnetic field, assuming a local approximation of $|B| \approx B_z$, typically consisting of regular solid spherical harmonics [19], generated by coils obtained by the target field method [20]. This method relies on the inversion of the Biot-Savart law, allowing us to determine the current distribution that best generates a desired magnetic

Table 1
A summary of the geometrical parameters of the flow setup as well as the NMR acquisition parameters.

Item	Description
Device Size	$125 \times 57 \times 15$ mm^3
Device Mass	0.205 kg
Detection Coil (VOI)	Stripline ($10 \times 7 \times 3$ mm^3)
Shimming Coil (VOI)	Biplanar ($10 \times 7 \times 3$ mm^3)
Transmitter Coil (VOI)	Solenoid (entire sample)
Flow Channel Size (VOI)	$27 \times 19 \times 3$ mm^3($10 \times 10 \times 3$)
Magnetic Field	1.05 T
Gradient Power	14165.19 Hz/mm
Gradient Duration	6 ms
First Acquisition Duration	0.2 ms
Second Acquisition Duration	12 ms
Sampling Frequency	50 kHz
RF Pulse Duration	0.0256 ms
RF Pulse Power	0.52 W
SNR	260

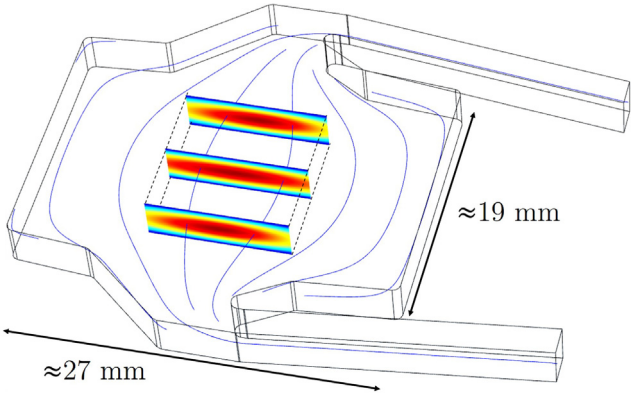

Fig. 3. Schematic of the flow channel and the expected streamlines of the fluid flow. The expected, idealised laminar-flow velocity profile along the channel is shown on three cross-sections of the VOI.

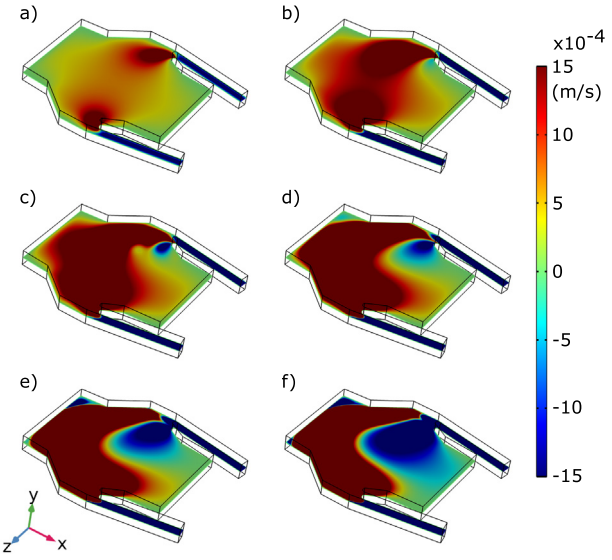

Fig. 4. Simulation results of the z-component of the flow field (indicating strongly varying out-of-plane flow) for different mass flow rates (a) 0.1, (b) 0.2, (c) 0.3, (d) 0.6, (e) 1.2, and (f) 2.0 kg/h.

field over a certain VOI. As a way to overcome the system's ill-conditioning, the dissipative power of the current density [16] was introduced as a regularisation term.

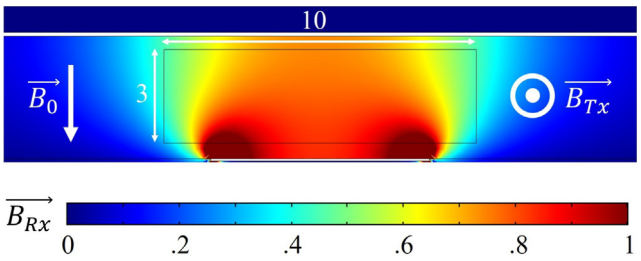

Fig. 5. Normalised sensitivity profile of the 7 mm wide stripline optimised for detection on the VOI. Directions of the main precession field, B_0, and the RF excitation field, B_{Tx}, are shown for clarity.

The implementation of a biplanar coil geometry was based on principles developed in [6]. The output of the method is a continuous distribution over the coil planes, which we discretised by taking level sets of the corresponding stream functions [3,15]. This routine was used for the design of seven shimming coils, and their simulated performance was quantified in Table 2.

To test the performance of the shims, the flow channel was filled and placed inside a commercial NMR imaging system (ICON, Bruker BioSpin) with its shim system disabled. Using the shim system developed and shown above, it was possible to drastically improve the unshimmed decay time ($\mathrm{FWHM}_{no\ shim} \approx 1/T_2^* = (1\ \mathrm{ms})^{-1} = 990$ Hz) to a far longer decay ($\mathrm{FWHM}_{shim} = (36\ \mathrm{ms})^{-1} = 28$ Hz) which enabled continuous measurement during the flow probing experiments. These had probing rates requiring two FID measurements in 100 ms, for example. Comparing the SNR obtained in the 36 ms decay to that of an ideal non-decaying signal in a 50 ms acquisiton, one obtains 58%, a value considered to be sufficient given the complexity of further marginal improvements. The shims required for the linewidth correction in Fig. 6 had a total power dissipation of 6 mW, corresponding to an adiabatic heating of stationary water in the flow channel of 93 μK in 50 ms, a negligible value even in a worst case scenario.

The aforementioned parts, devised to be assembled together, were then connected and prepared for measurement in a complete setup spanning 15x57x95 mm. To confirm the correct function of the system, a FLASH imaging sequence was used to measure the selection of the effect of the three components developed. Initially, the magnitude contrast allowed us to see how the major signal contribution was derived from proximity to the stripline. Its outline and the flow channel shape is visible in Fig. 7. As the spins dephased, only the spins on VOI remained coherent, due to selective behaviour of the shim system, and thus the response appeared to approximate well that of the desired near-2D flow.

4. Flow results

A functioning front-end, equipped with all the components to enable a flow velocimetry experiment, was combined with the pulse sequence of Fig. 8 to measure flow. All subsequent measurements were carried out in a 1T field (ICON, Bruker BioSpin). To have a robust phase response, a wideband excitation pulse was used to compensate for drift, which represents one the most important problems of low-field permanent magnets, in particular when the phase of the signal is used to extract the results. Despite the use of a drift adjustment step before each readout, such an excitation pulse is still necessary because the it cannot compensate the magnetic field precisely. Furthermore, frequency adjustment cannot be used since it changes the phase response of the spectrometer hardware, after which the results can no longer be correlated. The pulse sequence consisted of two acquisitions. The excitation pulse was followed by the first acquisition. The second

Table 2
Simulated performance of the seven spherical harmonic shims, for coil position z, the standard deviation E of the field relative to the shim, the power dissipated P_d per T/m or T/m^2,the total resistance R, the inductance [2] L, and the inductive rise time t_{LR}.

SH	z (mm)	E (ppm)	P_d (mW)	R (Ω)	L (μH)	t_{LR} (μs)
y	7.42	881	9.72	4.1	12	2.9
x	7.09	936	8.60	4.0	11	2.8
z	6.87	658	4.59	3.1	9.4	3.0
yz	6.56	617	18.6	1.4	2.6	0.5
xz	6.34	659	15.8	1.4	2.6	0.5
xy	6.04	756	396	2.4	3.9	0.6
$2z^2 - r^2$	5.82	327	24.9	3.2	6.3	0.5

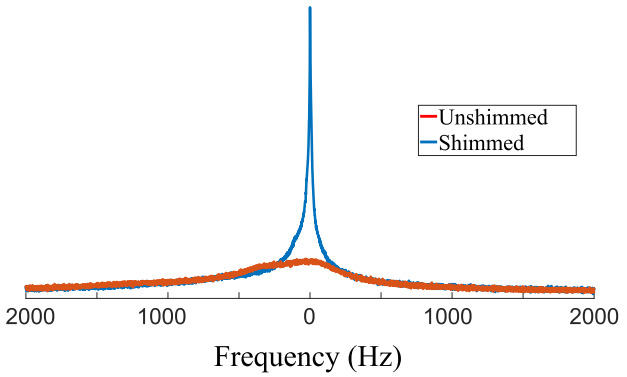

Fig. 6. Magnitude of the Fourier transform of two equal and sequential experiments with and without the shims enabled.

acquisition was preceded by a pair of bipolar gradients, resulting in a direct relationship between the velocity and the injected phase difference between the acquisitions. Because of the combined effects of T_2^*, eddy current, diffusion, and phase dispersion due to flow encoding, the signal of the second acquisition was much weaker than the first one. Different acquisition times needed to be used to balance the SNRs. The trade-off was designed based on the employed k_{enc}. Larger k_{enc}s necessitated a greater ratio between the second and first acquisition time. Regarding the bipolar gradients, as long as SNR was sufficient, it was better to use the stronger bipolar gradient which injected more phase, resulting in a better phase-velocity resolution and phase-SNR. Hence, a bipolar gradient with 6 ms pulse length and 14165.19 Hz/mm of power was used for this study.

The measurement was performed for 26 different flow rates ranging from 0 to 2 kg/h, and for 10 repetitions for each point. A flow system was set up using a pressure control system (OB1 MkIII+, Elveflow) with a stated pressure stability of 0.006% FS, well below the precision of common flow measurements. This meant that the flow could be considered to be steady-state for the duration of the measurement. Given the unknown hydraulic resistance of the setup, a high-precision Coriolis flowmeter (mini CORI-FLOW M13, Bronkhorst®) was used to benchmark the flow results at a precision of 0.2%. The current setup was designed based on a bipolar gradient technique, yielding the volumetric flow of the fluid. The density of the fluid was taken into account to compare these results with those of a Coriolis flowmeter, which yields the mass flow rate.

The experimental results, shown in Figs. 9 and 11, were in a very good agreement with the phase response of Fig. 1, as long as the flow followed the simulation profile shown in Fig. 4. In the other words, the injected phase linear depended on flow until $k_{enc}\overline{v} \approx 2.7$ which corresponded to a mass flow rate of 0.25 kg/h. The phase experienced a maximum at 0.30 kg/h, after which there was a downward non-linear trend. The expected model breakdown was caused by the flow response introduced in Fig. 4, showing a

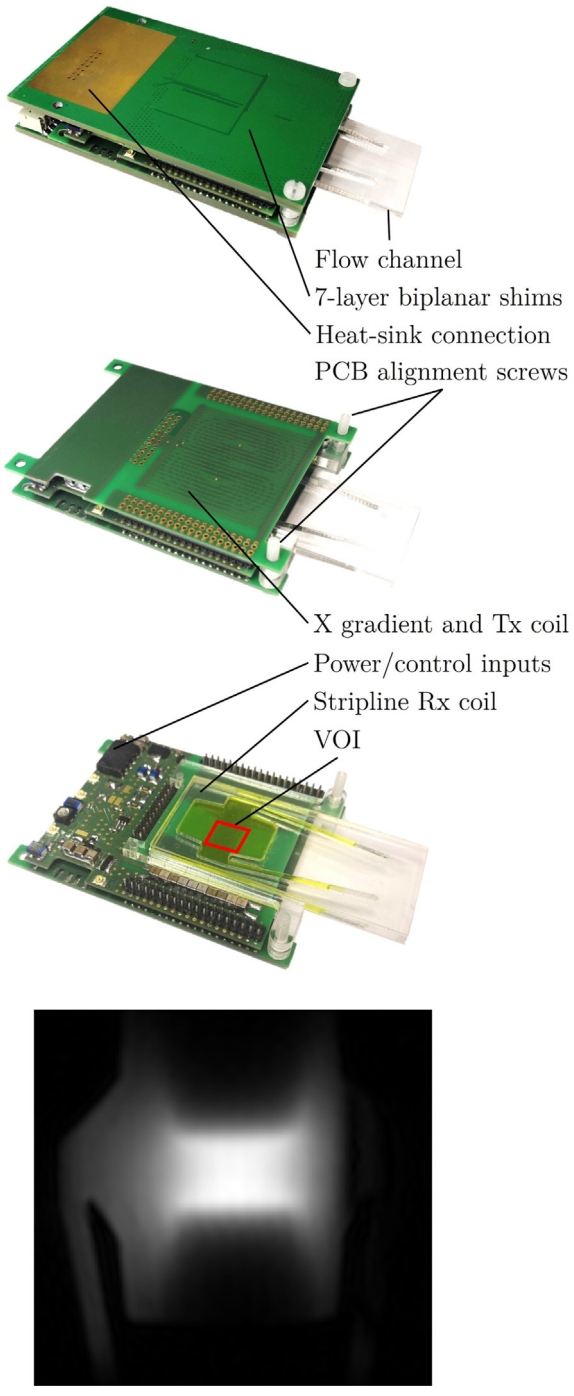

Fig. 7. Sequential disassembly steps of the flow measurement setup used for the experiment, with the third photo indicating the VOI with a red frame. The static no-flow MRI image shows the dominance of the VOI signal.

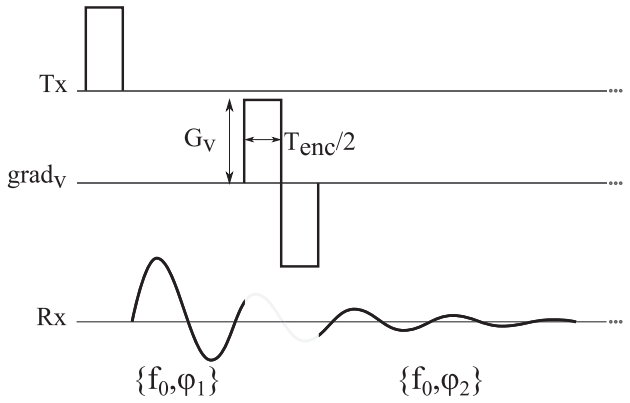

Fig. 8. Pulse sequence used to encode flow into phase, establishing $k_{enc} = \gamma G_v T_{enc}^2/4$ to obtain the phase difference $\phi = \varphi_2 - \varphi_1$.

recirculation region in the flow channel before 0.30 kg/h, which affected flow behaviour in the detection region and resulted in a reduction in the injected phase. As the flow rate increased, the recirculation region expanded into the VOI and at 1.2 kg/h, the positive and negative z-components completely cancelled each other out, resulting in a vanishing injected phase. Nonetheless, despite the deviation from the model, results showed that the setup could still be used to measure the flow rate. For our particular geometry, because the flow pattern changed at 0.3 kg/h, the setup could be used to measure the flow also for faster flows, as long as the model's progression in Fig. 9 was accounted for in a look-up table.

In order to evaluate the precision of the current method, a comparison between experimental results of the current setup, and that of Bronkhorst® flow meter, is made and shown in Fig. 10. The results from both setups are in good agreement up to 600 mbar (corresponding to 0.25 kg/h). Beyond that, the results diverge, since the flow behaviour loses ideal conditions in the flow channel.

Regarding the amplitude of the signal shown in Fig. 11, despite the fact that in theory it showed a sinusoidal downward trend, there was an upward trend at the beginning of the measured curve which was not expected. It appeared that another unknown effect lead to phase dispersion, and the phase dispersion due to flow encoding compensated the effect up to $k_{enc}\overline{v} \approx 1$, which corresponded to a mass flow rate of 0.09 kg/h. The reason could be diffusion, eddy currents, or, most probably, a small asymmetry in the bipolar gradient. In fact, to some extent, the superposition of this unknown effect with flow effects lead to better in-phase signals for part of the range, and at higher velocities a sinusoidal downward trend in the amplitude of the signal was observed.

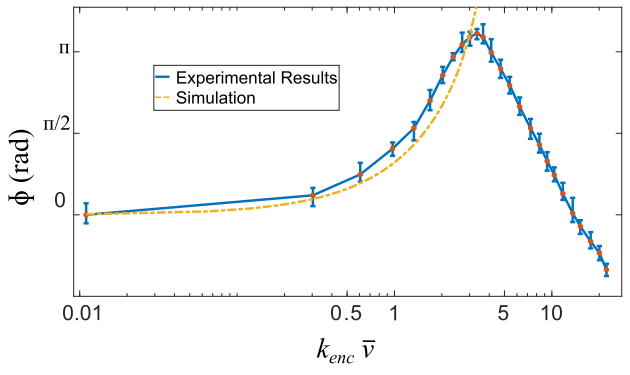

Fig. 9. Comparison between simulation and experimental results for the injected phase vs. mass flow rate (error bar is plotted for 10 different measurements).

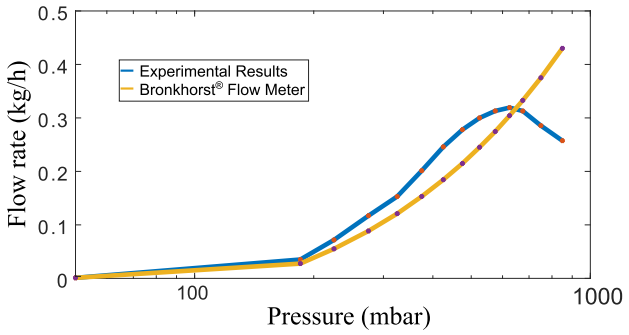

Fig. 10. Comparison between experimental results of the current setup and Bronkhorst® flow meter.

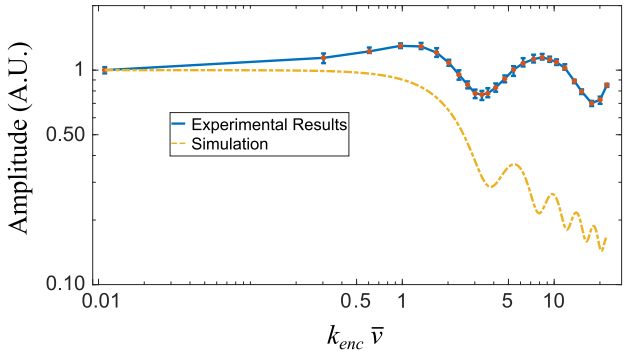

Fig. 11. Comparison between simulation and experimental results for the magnitude of the second acquisition vs. mass flow rate (error bar is plotted for 10 different measurements).

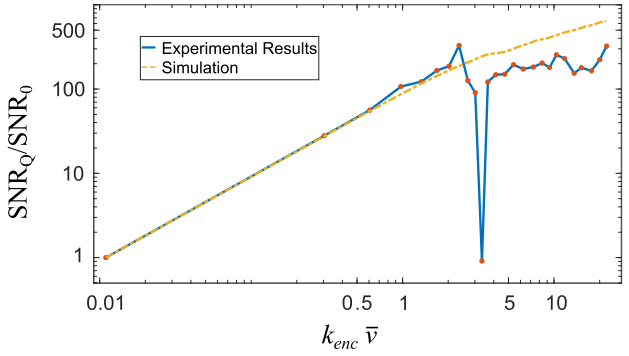

Fig. 12. Comparison between simulation and experimental results for SNR vs. mass flow rate based on Eq. (2).

5. Conclusions

In this manuscript, a phase-encoding method was proposed for an NMR based flowmeter, showing a theoretical upper bound *above that of the NMR measurement itself*, thus confirming that a near-2D net-phase flow encoding method can outperform concepts based on cylindrical flow, and without suffering the amplitude loss of magnitude-based flow encoding solutions (See Fig. 12). At the same time, on the more practical side, we could show that this idea can be implemented using low cost techniques, which would facilitate translation into a product. Our concept relies on an NMR front-end, depicted in Fig. 7, which could be built and integrated into a standard gap/C-shaped magnet for an overall pricetab that remains under 1000€, i.e. using standard electronics and mechan-

ical construction, and (in hindsight) requiring about a fortnight of implementation effort.

Together, these advances thus demonstrate how the phase-encoding approach shown in Fig. 1, based on engineered flow profiles, open the door to the simplification of NMR flowmeters, while showing several advantages when compared to magnitude-based methods:

- *Improved SNR:* the results in Fig. 2 introduce two new clear advantages past the current state of the art. Initially, introduce the SNR advantage of highly phase-wrapped encodings versus standard $-\pi$ to π approaches. Simultaneously, they show how the engineering of a 2D flow accesses a larger SNR when compared to cylindrical flow, all while remaining fully compatible with standard NMR methods.
- *Large locally-bijective domain:* similar to what is expected from an ideal plug flow, but very different from what would be achievable in cylindrical flow, the 2D flows show a continually non-zero amplitude of their response. This property, while appearing trivial at first, as one could in principle adjust k_{enc} for a non-zero value of the response of cylindrical flow, means that a continually and locally-bijective correspondence of phase to velocity exists. At high phase wrapping numbers, where a small change in the average velocity implies a large behavioural change, one does not run the risk of a missed measurement, which allows for the continuous tracking of velocity/wrapping numbers, even in highly dynamic flow.
- *Velocity independence:* the theoretical framework which establishes a function of $k_{enc}\overline{v}$, instead of simply $\overline{v}$, allows for an encoding process that is fully velocity independent as long as k_{enc} can be adequately adjusted. This contrasts with the low-turndown ratio of magnitude-based methods, which do not have this freedom. This adjustment further allows one to leverage the increasing statistical significance of measurements at large $k_{enc}\overline{v}$ up to the upper and lower bounds of k_{enc}, or up until when secondary effects become limiting.

The main limitation of this method is that it is not easily applicable to fluids with very small gyromagnetic ratio. Its main potential is that spectrometry and flow metering can be conveniently combined, which sets it apart from other approaches. We therefore expect that several interesting developments can be expected in this field. Having a custom flow chamber is one of the promising directions. Despite the fact that the current setup has a limited range of measurable flow, it is readily feasible to highly increase the range using the same technique. A 2D-like flow profile for a wider range of flow rates would push forward the limit. Also, in case a bigger volume is required for the chamber, a similar setup at a larger scale can be used. It is not necessary to have laminar flow in the detection area (FOV). However, having it will lead to a higher SNR. Turbulent flow will still lead to a correct measurement, as long as a locally bijective relationship exists between flow rate and the injected phase. Another topic for further studies can be multiphase flow measurement, by exploiting signals from nuclei with differing chemical shift.

Declaration of Competing Interest

The authors declare that they have no known competing financial interests or personal relationships that could have appeared to influence the work reported in this paper.

Acknowledgements

PFS acknowledges Bürkert GmbH & Co. KG for funding for his part of this project. JGK, MAJ and MJ acknowledge partial support from the European Union's Future and Emerging Technologies Framework (H2020-FETOPEN-1-2016-2017-737043-TISuMR). JGK, MJ and MC acknowledge the DFG for partial funding [Contract KO 1883/29-1].

References

[1] L.A. Colnago, F.D. Andrade, A.A. Souza, R.B.V. Azeredo, A.A. Lima, L.M. Cerioni, T. M. Osán, D.J. Pusiol, Why is Inline NMR Rarely Used as Industrial Sensor? Challenges and Opportunities, Chem. Eng. Technol. 37 (2014) 191–203, https://doi.org/10.1002/ceat.201300380.
[2] R. Dengler, Self inductance of a wire loop as a curve integral, Adv. Electromagn. 5 (2016) 1–8, https://doi.org/10.7716/aem.v5i1.331.
[3] W.A. Edelstein, F. Schenck, Current streamline method for coil construction. US Patent 4,840,700, 1989.
[4] C.J. Elkins, M. Markl, N. Pelc, J.K. Eaton, 4d magnetic resonance velocimetry for mean velocity measurements in complex turbulent flows, Exp. Fluids 34 (2003) 494–503, https://doi.org/10.1007/s00348-003-0587-z.
[5] F. Deng, C. Xiong, S. Chen, G. Chen, M. Wang, H. Liu, J. Zhang, D. Xu, Y. Tao, L. Xiao, A method and device for online magnetic resonance multiphase flow detection, Petrol. Explor. Developm. 47 (2020) 855–866, https://doi.org/10.1016/S1876-3804(20)60101-x.
[6] L.K. Forbes, S. Crozier, Novel target-field method for designing shielded biplanar shim and gradient coils, IEEE Trans. Magn. 40 (2004) 1929–1938, https://doi.org/10.1109/TMAG.2004.828934.
[7] E. Fukushima, Nuclear magnetic resonance as a tool to study flow, Annu. Rev. Fluid Mech. 31 (1999) 95–123, https://doi.org/10.1146/annurev.fluid.31.1.95.
[8] L.F. Gladden, A.J. Sederman, Recent advances in Flow MRI, J. Magn. Reson. 229 (2013) 2–11, https://doi.org/10.1016/j.jmr.2012.11.022.
[9] P. Lauterbur, Image formation by induced local interactions: examples employing nuclear magnetic resonance, Nature 242 (1973) 190–191, https://doi.org/10.1038/242190a0.
[10] M. Appel, J.J. Freeman, D. Pusiol, Robust multi-phase flow measurement using magnetic resonance technology, Soc. Petrol. Eng. (2011), https://doi.org/10.2118/141465-MS.
[11] P. Mansfield, P.K. Grannell, NMR 'diffraction' in solids, J. Phys. C: Solid State 6 (1973) L422–L426, https://doi.org/10.1088/0022-3719/6/22/007.
[12] O.C. Morse, J.R. Singer, Blood Velocity Measurements in Intact Subjects, Science 170 (1970) 440–441, https://doi.org/10.1126/science.170.3956.440.
[13] K.T. O'Neill, A. Klotz, P.L. Stanwix, E.O. Fridjonsson, M.L. Johns, Quantitative multiphase flow characterisation using an earth's field nmr flow meter, Flow Meas. Instrum. 58 (2017) 104–111, https://doi.org/10.1016/j.flowmeasinst.2017.10.004.
[14] T. Osán, J. Ollé, M. Carpinella, L. Cerioni, D. Pusiol, M. Appel, J. Freeman, I. Espejo, Fast measurements of average flow velocity by low-field 1h nmr, J. Magn. Reson. 209 (2011) 116–122, https://doi.org/10.1016/j.jmr.2010.07.011.
[15] G.N. Peeren, Stream function approach for determining optimal surface currents, J. Comput. Phys. 191 (2003) 305–321, https://doi.org/10.1016/S0021-9991(03)00320-6.
[16] M. Poole, R. Bowtell, Novel gradient coils designed using a boundary element method, Concepts Magn. Reson. Part B: Magn. Reson. Eng. Educ. J. 31 (2007) 162–175, https://doi.org/10.1002/cmr.b.20091.
[17] S.J. Richard, B. Newling, Measuring flow using a permanent magnet with a large constant gradient, Appl. Magn. Reson. 50 (2019) 627–635, https://doi.org/10.1007/s00723-018-1107-x.
[18] P.F. Silva, M. Jouda, J.G. Korvink, Geometrically-differential NMR in a stripline front-end, J. Magn. Reson. 310 (2019) 106659, https://doi.org/10.1016/j.jmr.2019.106659, URL: https://doi.org/10.1016/j.jmr.2019.106659https://linkinghub.elsevier.com/retrieve/pii/S1090780719302988.
[19] E. Steinborn, K. Ruedenberg, Rotation and translation of regular and irregular solid spherical harmonics, in: Advances in quantum chemistry, vol. 7, Elsevier, 1973, pp. 1–81. doi: 10.1016/S0065-3276(08)60558-4.
[20] R. Turner, A target field approach to optimal coil design, J. Phys. D: Appl. Phys. 19 (1986) L147, https://doi.org/10.1088/0022-3727/19/8/001.